Structural, chemical and magnetic properties of secondary phases in Co-doped ZnO

Ney, A; Kovács, András; Ney, V; Ye, S; Ollefs, K; Kammermeier, T; Wilhelm, F; Rogalev, A; Dunin-Borkowski, Rafal E.

Published in:
New Journal of Physics

Link to article, DOI:
10.1088/1367-2630/13/10/103001

Publication date:
2011

Document Version
Publisher's PDF, also known as Version of record

Structural, chemical and magnetic properties of secondary phases in Co-doped ZnO

2011 New J. Phys. 13 103001

(http://iopscience.iop.org/1367-2630/13/10/103001)

New Journal of Physics
The open-access journal for physics

Structural, chemical and magnetic properties of secondary phases in Co-doped ZnO

A Ney[1,5], A Kovács[2,4], V Ney[1], S Ye[1], K Ollefs[1], T Kammermeier[1], F Wilhelm[3], A Rogalev[3] and R E Dunin-Borkowski[2,4]

[1] Fakultät für Physik and CeNIDE, Universität Duisburg-Essen, Lotharstrasse 1, D-47057 Duisburg, Germany
[2] Center for Electron Nanoscopy, Technical University of Denmark, DK-2800 Kgs Lyngby, Denmark
[3] European Synchrotron Radiation Facility (ESRF), 6 Rue Jules Horowitz, BP 220, 38043 Grenoble Cedex, France
[4] Ernst Ruska-Centre for Microscopy and Spectroscopy with Electrons, Peter Grünberg Institute, Research Centre Jülich, D-52425 Jülich, Germany
E-mail: andreas.ney@uni-due.de

New Journal of Physics **13** (2011) 103001 (17pp)
Received 20 June 2011
Published 3 October 2011
Online at http://www.njp.org/
doi:10.1088/1367-2630/13/10/103001

Abstract. We have utilized a comprehensive set of experimental techniques such as transmission electron microscopy (TEM) and synchrotron-based x-ray absorption spectroscopy (XAS) and the respective x-ray linear dichroism and x-ray magnetic circular dichroism to characterize the correlation of structural, chemical and magnetic properties of Co-doped ZnO samples. It can be established on a quantitative basis that the superparamagnetic (SPM) behavior observed by integral superconducting quantum interference device magnetometry is not an intrinsic property of the material but stems from precipitations of metallic Co. Their presence is revealed by TEM as well as XAS. Annealing procedures for these SPM samples were also studied, and the observed changes in the magnetic properties found to be due to a chemical reduction or oxidation of the metallic Co species.

[5] Author to whom any correspondence should be addressed.

Contents

1. Introduction

In the past ten years, dilute magnetic semiconductors (DMS) based on oxide materials, and $Zn_{1-x}Co_xO$ (Co : ZnO) in particular, have raised high expectations as potentially exhibiting room temperature ferromagnetism [1]. Since the first report [2] of ferromagnetism in Co : ZnO, sample quality and reproducibility have been issues, giving rise to a long sequence of controversial publications, captured in many review articles (see, e.g., [3, 4]). An elegant approach towards identifying the relevant mechanism for magnetic order in Co : ZnO is annealing experiments. It was shown that annealing Co : ZnO in a Zn (oxygen) atmosphere could reversibly switch on (off) the magnetic order, which was correlated with the increase (decrease) of the n-type carrier concentration [5]. In contrast, Zn-annealing had only a small, possibly extrinsic, influence on the magnetic properties of Co-ion-implanted ZnO substrates [6]. Despite the persisting controversy [4], there is increasing experimental evidence that phase-pure Co : ZnO is intrinsically paramagnetic (PM) [3] with antiferromagnetic Co–O–Co interactions [7, 8]. This conclusion is independent of the n-type carrier concentration as long as the structural integrity is maintained, as recently demonstrated for Al-codoped Co : ZnO [9]. In particular, the use of synchrotron-based experimental techniques such as x-ray absorption spectroscopy (XAS), and x-ray linear dichroism (XLD) and x-ray magnetic circular dichroism (XMCD), constitutes a powerful toolbox for a meaningful characterization of DMS materials [10]. For Co : ZnO, XAS in the hard x-ray regime has proven to be particularly useful in establishing quantitative quality indicators to discriminate between phase-pure samples and the onset of phase separation [11]. In contrast, when using soft x-rays the results remain less conclusive. Integral superconducting quantum interference device (SQUID) magnetometry and element-specific magnetometry using XMCD reveal a different magnetic behavior, i.e. the SQUID suggests ferromagnetism while the XMCD finds PM behavior of the Co [12]. Other authors report the absence of any remanent soft XMCD signal at any absorption edge of each atomic species of Co : ZnO [13]. To account for these puzzling findings, the presence of defects in Mn-doped ZnO was correlated with the observed ferromagnetism [14, 15], a conclusion

that was recently corroborated by a novel theoretical explanation [16]. Usually, the long-range magnetic order is only evidenced by SQUID, e.g., in [2, 12, 13, 15]. On the other hand, the presence of long-range magnetic order seen by SQUID could be correlated with the presence of metallic Co precipitations using a combination of extended x-ray absorption fine-structure spectroscopy (EXAFS) and transmission electron microscopy (TEM) [17] on polycrystalline samples and, for epitaxial films, using soft XMCD and TEM [18] or a combination of soft and hard x-rays [19]. Therefore, the microscopic origin of long-range magnetic order in Co : ZnO is still under debate; hence further experimental efforts are necessary to unambiguously identify the microscopic origin of the magnetic order seen in integral SQUID magnetometry.

Here we present a comprehensive study based on a combination of TEM, XAS and SQUID to investigate the structural and magnetic properties of PM Co : ZnO samples in comparison with superparamagnetic (SPM) samples. The XAS quality indicators that were established earlier [11] will be correlated with an in-depth TEM analysis highlighting the high structural quality of epitaxial PM Co : ZnO films. In addition, the structure of SPM samples and the influence of annealing procedures on the magnetic properties can provide insight into the microscopic origin of the magnetic response in SPM Co : ZnO samples. The annealing experiments confirm that the changes in the magnetic properties are not due to a change in the carrier concentration but due to a reduction (oxidation) of a fraction of the Co that is not substitutionally incorporated into the ZnO host crystal, corroborating earlier findings on polycrystalline Co : ZnO samples annealed in hydrogen [20]. In all the studied cases, the magnetic behavior as measured with integral SQUID magnetometry at room temperature can be quantitatively correlated with the low-temperature magnetic response in element selective $M(H)$-curves measured by XMCD at photon energies characteristic of metallic Co, thus pointing toward an extrinsic origin of the magnetic order in the SPM Co : ZnO samples.

2. Experimental details

The aim of this section is twofold. Firstly, a brief overview of the experimental techniques used will be given. Secondly, the preparation details and existing pre-characterization of all sample specimens presented in this paper will be provided.

2.1. Experimental techniques

The integral structural properties were routinely characterized by x-ray diffraction (XRD), which reveals for PM samples a c-plane orientation for the ZnO films and no indication of additional crystallographic phases within the detection limit of XRD, i.e. ruling out Co crystallites above $\sim$2–4 nm diameter; cf [18]. For SPM samples, additional reflections were observed in some cases [11].

For TEM investigations, cross-sectional samples of Co : ZnO films were fabricated by mechanical polishing and Ar ion milling. Each cross-sectional specimen was finished by low-energy Ar ion milling at 500 eV in order to minimize sample damage. For a conventional TEM characterization, an FEI Tecnai G2 microscope was used at 200 kV. Both image and probe aberration-corrected TEM and scanning TEM (STEM) studies were carried out using FEI Titan microscopes operated at 300 kV. Information about the local concentration of the elements was obtained using a combination of STEM images and energy dispersive x-ray spectroscopy (EDS) line-scan and point probe experiments.

The XAS spectra in the near edge regime (XANES) were taken at the ID12 beamline [21] of the ESRF in total fluorescence yield. The XANES/XLD measurements were carried out at 300 K and a quarter wave plate [21] was used to flip the linear polarization of the synchrotron light from vertical ($E \parallel c$) to horizontal ($E \perp c$); the angle of incidence was 10° with respect to the sample surface. The XLD was taken as the direct difference of the normalized XAS with $E \perp c$ and $E \parallel c$. The isotropic XANES was derived from the weighted average of the two XAS spectra, i.e. $(2 \times \mathrm{XAS}(E \perp c) + \mathrm{XAS}(E \parallel c))/3$. Note that in the case of perfectly c-oriented samples, this corresponds to the true isotropic XANES. The XMCD measurements were taken at 6.5 K as the direct difference of normalized XANES spectra recorded with right and left circular polarized light for $H = 6$ T under grazing incidence (15°), respectively. To minimize artifacts, the direction of the external magnetic field was reversed as well. For c-oriented samples the XANES in this case corresponds to $(\mathrm{XAS}(E \perp c) + \mathrm{XAS}(E \parallel c))/2$.

The integral magnetic measurements were carried out in the temperature range from 5 to 300 K using a commercial SQUID magnetometer (Quantum Design MPMS-XL 5 T) taking great care to minimize magnetic contamination and sample-mounting related artifacts [22, 23]. The magnetic field was applied in the sample plane, and no correction of the residual magnetic field as described in [23] was done. This led to a small residual magnetic hysteresis limiting the significant magnetic signal size to above $2\text{–}4 \times 10^{-7}$ emu; smaller signals were disregarded [22, 23]. A standard SQUID measurement cycle in this work consists of $M(H)$ curves recorded at 300 and 5 K and two $M(T)$ measurements while warming from 5 to 300 K in 10 mT: once under field-cooled (FC; in 4 T) conditions and once under zero-field-cooled (ZFC) conditions. The diamagnetic background of the substrate was determined from the $M(H)$ behavior at 300 K and high magnetic fields, and it is subsequently subtracted from all magnetization data.

Throughout this paper the magnetic properties, along with the sample names, are termed either 'PM' or 'SPM'. The term 'ferromagnetic' (FM) is avoided. PM samples refer to the absence of any magnetic hysteresis at any temperature down to 5 K, coinciding FC versus ZFC curves and a pronounced 'Brillouin-like' $M(H)$ curve at low temperatures. SPM samples are characterized by hysteretic $M(H)$ behavior at low temperatures, a clear separation of the FC versus ZFC curves with a characteristic maximum in the ZFC data typical of blocking behavior and mostly anhysteretic but S-shaped $M(H)$ curves at 300 K indicative of large magnetic 'supermoments'.

It should be stressed that SPM behavior in Co : ZnO can have various different microscopic origins and the experimental challenge is to discriminate between them. On the one hand, if the magnetic order in DMS materials can be described by a coalescence model, e.g., of bound magnetic polarons as in [27], SPM-like signatures in integral magnetometry are likely. The 'blocking temperature', e.g., would correspond to the temperature where the magnetic coupling between the magnetic polarons sets in or breaks down, respectively. In this scenario, SPM is an *intrinsic* property of the material. On the other hand, small ferromagnetic inclusions naturally constitute SPM behavior. Such 'nanoclusters' can have different microscopic origins: (i) phase separation of dopant atoms forming secondary phases, (ii) decoration of grain boundaries with dopant atoms beyond the solubility limit, (iii) magnetic contaminations due to sample-handling and (iv) dopant-rich regions in a dopant-poor host matrix, often termed 'spinodal decomposition'. Whereas (iv) can be considered as an *intrinsic* property of the material, (i)–(iii) should be regarded as *extrinsic*. Only in the cases where scenarios (i)–(iii) are experimentally

ruled out, (iv) or a bound magnetic polaron scenario remains the possible explanation for the magnetic behavior of DMS materials.

2.2. Sample overview

Nominally 10% Co : ZnO films were grown on epiready *c*-plane sapphire substrates using reactive dc-magnetron sputtering (RMS) at 20 W from Co/Zn metal targets in an ultrahigh vacuum deposition system with a base pressure of 5×10^{-10} mbar. The pressure during deposition was 4×10^{-3} mbar at a substrate temperature of 350 °C. The composition of the Ar : O_2 sputter gas was varied from 10 : 1, leading to PM Co : ZnO samples down to 10 : 0.5 yielding SPM behavior [11]. The **PM-RMS** sample was previously studied using SQUID only and it was shown to exhibit anisotropic paramagnetism (see figure 3 in [24]), which can be described by an effective spin model with single ion anisotropy introduced for Co^{2+} impurities in ZnO [25] and later used for epitaxial Co : ZnO films [26]. The **SPM-RMS** sample was studied before using SQUID and XAS [11]. For this work the sample was split into three pieces. One remained in the as-grown state (**as-g**) in which it was studied before, one was annealed under high vacuum conditions ($p \sim 10^{-6}$ mbar) at 450 °C for 30 min (**HV-a**) and one was annealed in oxygen atmosphere at 450 °C for 30 min (**O_2-a**). It should be stressed that identical findings were found in another SPM sample grown with an Ar : O_2 ratio of 10 : 0.4; for better comparability with previously published data, we have chosen to present the annealing data from the sample in [11]. In addition, a nominally 15% Co : ZnO film was grown with an Ar : O_2 ratio of 10 : 0.5 (**SPM-RMS** 15% sample). TEM cross-sectional samples were fabricated from the PM-RMS and the SPM-RMS as-g samples, respectively.

In addition, an SPM nominally 5% Co : ZnO sample was grown by pulsed laser deposition (PLD) on *r*-plane sapphire in three steps at growth temperatures of 600, 400 and 200 °C at the Johannes–Gutenberg University in Mainz. The preparation concept for this **SPM-PLD** sample was intended to maximize the magnetic response of similar Co : ZnO samples that were studied earlier [13, 28]. Note that for this sample the geometry for the XLD measurements had to be altered to normal incidence of the x-ray beam with suitable azimuthal orientation to ensure that $E \perp c$ and $E \parallel c$, respectively.

As a reference material for the size of the XLD at the Zn *K*-edge, an undoped 305(1) nm thick ZnO epitaxial layer was grown on a 20 nm Mg : ZnO buffer layer on *c*-plane sapphire substrates by molecular beam epitaxy (MBE) at the Walter Schottky Institute controlling the growth using reflection high-energy electron diffraction. It has excellent structural quality as indicated by the full-width at half-maximum (FWHM) of 0.007° in ω-rocking curves of the (0002) reflection of ZnO, which itself has an FWHM of 0.03° in the ω–2θ-scan.

3. Experimental results

The presentation of the experimental results is organized as follows. First, the TEM investigations of the PM-RMS and the SPM-RMS samples are compared. The integral magnetic properties of the SPM-RMS sample are determined as a function of the annealing treatment. Subsequently, the XANES, XLD and XMCD results for all samples are presented. This is complemented by a detailed XANES analysis of the different Co-species found in the SPM samples. Finally, the element-selective magnetic properties are compared to integral SQUID magnetometry.

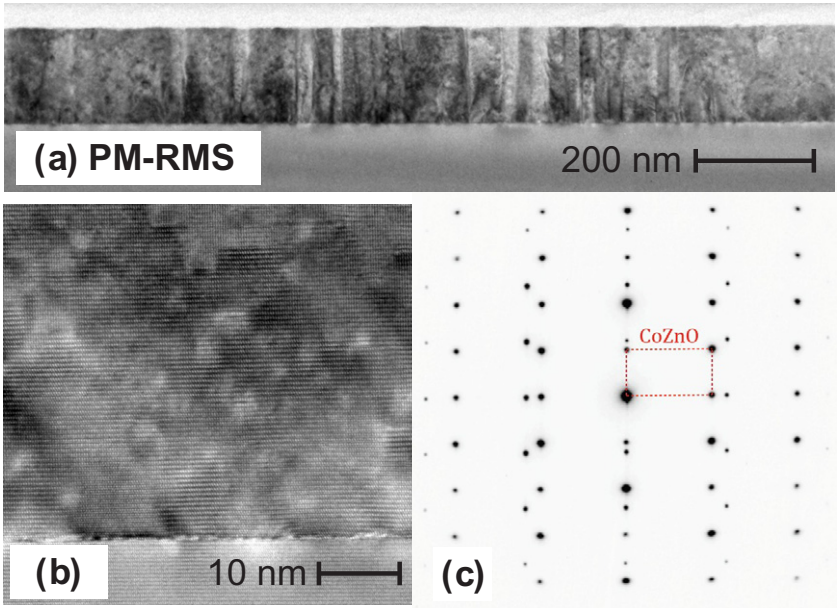

Figure 1. Bright-field TEM image of the PM-RMS sample at low (a) and higher (b) magnification, revealing a columnar structure of the film (a) as well as the high crystallinity of individual columns (b), which is further corroborated by the SAED in (c).

3.1. Structural properties measured by transmission electron microscopy (TEM)

Figure 1 summarizes the TEM investigations of the PM-RMS sample. The bright-field TEM image at low magnification in figure 1(a) reveals the columnar structure of the Co : ZnO film where the individual columns are highly oriented and have an average diameter of ∼40 nm. The film thickness is 158 nm with a very smooth surface. The enlarged bright-field image in figure 1(b) demonstrates the good crystalline quality within the individual columns, which is further corroborated by the selective area electron diffraction (SAED) pattern in figure 1(c) exhibiting rather sharp diffraction spots consistent with a highly epitaxial, *c*-oriented Co : ZnO layer. High-angle annular dark field images (HAADF; not shown) indicate a chemically homogeneous composition of the film. The wavy contrast at the interface to the sapphire substrate seen in figures 1(a) and (b) indicates a strain field at the interface. Strain fields within the Co : ZnO layer are also visible and the related defects will be discussed in more detail elsewhere. Overall, the TEM investigations demonstrate the good crystalline quality of the PM-RMS sample.

The TEM images of the SPM-RMS sample shown in figure 2 are in stark contrast to the PM-RMS sample. The low magnification in figure 2(a) reveals the globular structure of the film with a thickness of ∼160–190 nm, i.e. a very rough surface. The presence of many small crystallites in almost arbitrary orientation is especially seen in the top part of the film. Close to the interface, some grains are well oriented with respect to the substrate, as can be seen in figure 2(b), presumably giving rise to a weakly preferential crystallographic orientation of the layer. The polycrystalline structure of the SPM-RMS sample is highlighted by the SAED pattern in figure 2(c) exhibiting a spotty, but ring-like diffraction pattern. It is important to note that the microstructure of this sample is rather porous with a high density of grain boundaries. Note that

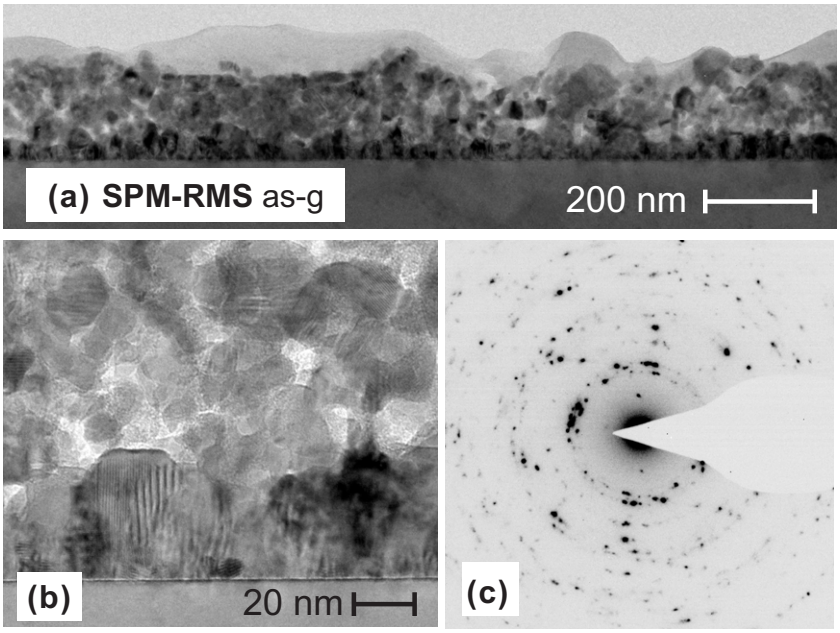

Figure 2. Bright-field TEM image of the SPM-RMS sample at low (a) and higher (b) magnification, revealing the globular structure of the film. The polycrystallinity is further demonstrated by the spotty SAED ring pattern (c).

this SPM-RMS sample yields an FWHM of the ZnO(002) reflection of 0.39° and an additional reflection indicative of ZnO(101) [11].

3.2. Annealing of the superparamagnetic, reactive magnetron sputtering (SPM-RMS) sample

Figure 3 summarizes the integral magnetic properties of the SPM-RMS sample using SQUID magnetometry for three different states of the SPM-RMS sample. To compare the three different pieces of identical film and substrate thickness, the SQUID data were normalized with respect to each other using the diamagnetic response, which is proportional to the sample area. The resulting data can thus be quantitatively compared with each other. In the as-grown state (SPM-RMS as-g, black squares) the high-field behavior in figure 3(a) reveals curved $M(H)$ behavior at 5 K, which is hysteretic at low fields; see figure 3(b). At 300 K the $M(H)$ curve is anhysteretic with a pronounced S-shape and a saturation value of 1.28×10^{-5} emu; see figure 3(c). The respective $M(T)$ behavior in the FC versus ZFC experiment in figure 3(d) is clearly indicative of SPM with a maximum of the ZFC curve around 200 K. This characteristic SPM behavior in the as-grown state is further enhanced by annealing the sample in high vacuum, as shown in figure 3 (SPM-RMS HV-a, red circles). The saturation value at 300 K increased to 2.17×10^{-5} emu, i.e. roughly by a factor of two; see figure 3(a). Also the hysteresis at 5 K is larger (b) and is still visible up to 300 K (c), which is consistent with a separation of the FC versus ZFC curves up to 300 K (d). Also, the maximum in the ZFC curve is shifted to higher temperatures. In contrast, the SPM-RMS sample annealed under oxygen atmosphere (SPM-RMS O_2-a, green triangles) shows PM behavior. The saturation value at 300 K visible in figure 3(a) is about 3×10^{-7} emu, i.e. close to the detection limit of the SQUID for such samples [22]. No hysteresis is visible at 5 K (b) or 300 K (c) and the FC versus ZFC curves

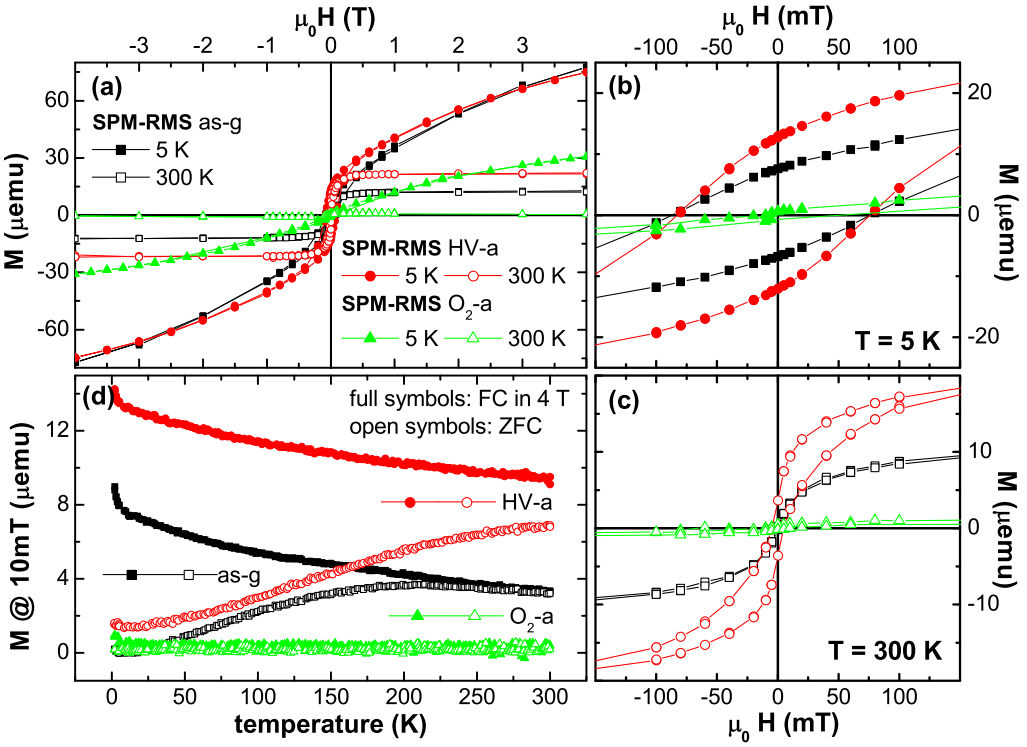

Figure 3. (a) $M(H)$ curves measured by SQUID on the SPM-RMS sample at 300 K (open symbols) and 5 K (full symbols) in the as-grown state (black squares) and after annealing under high-vacuum (red circles) and oxygen atmosphere (green triangles). The low field behavior is enlarged for the 5 K (b) and 300 K (c) data. Panel (d) summarizes the $M(T)$ curves recorded in 10 mT while warming under FC (full symbols) and ZFC (open symbols) conditions for the respective samples.

coincide (d). At first sight, the vanishing of SPM in this sample upon oxygen annealing is identical to previous reports [5], which was attributed to carrier-induced magnetic order in Co : ZnO. However, for this sample XANES, XLD and XRD measurements have already indicated possible phase separation [11] and the TEM investigation as shown in figure 2 underlines concerns about the phase purity of this sample. The actual microscopic origin of the SPM behavior will be discussed in more detail below.

3.3. Characterization using x-ray absorption spectroscopy

Figure 4 compiles all the measurements of XANES and respective XLD and XMCD at the Zn and Co K-edges of all specimens discussed in this paper. To assess the crystalline quality complementary to the TEM investigations, we first discuss the XLD at the Zn K-edge, which is indicative of the degree of crystalline order of the host ZnO matrix on a local scale. The XLD stems from the splitting of the unoccupied electronic states due to the crystal field of the surrounding atoms of the absorbing atom. In a first step, a maximum size of the XLD at the Zn K-edge shall be established, which is indicative of high crystalline perfection. For that purpose, a high-quality MBE-grown undoped ZnO layer was measured and is shown as a dark yellow

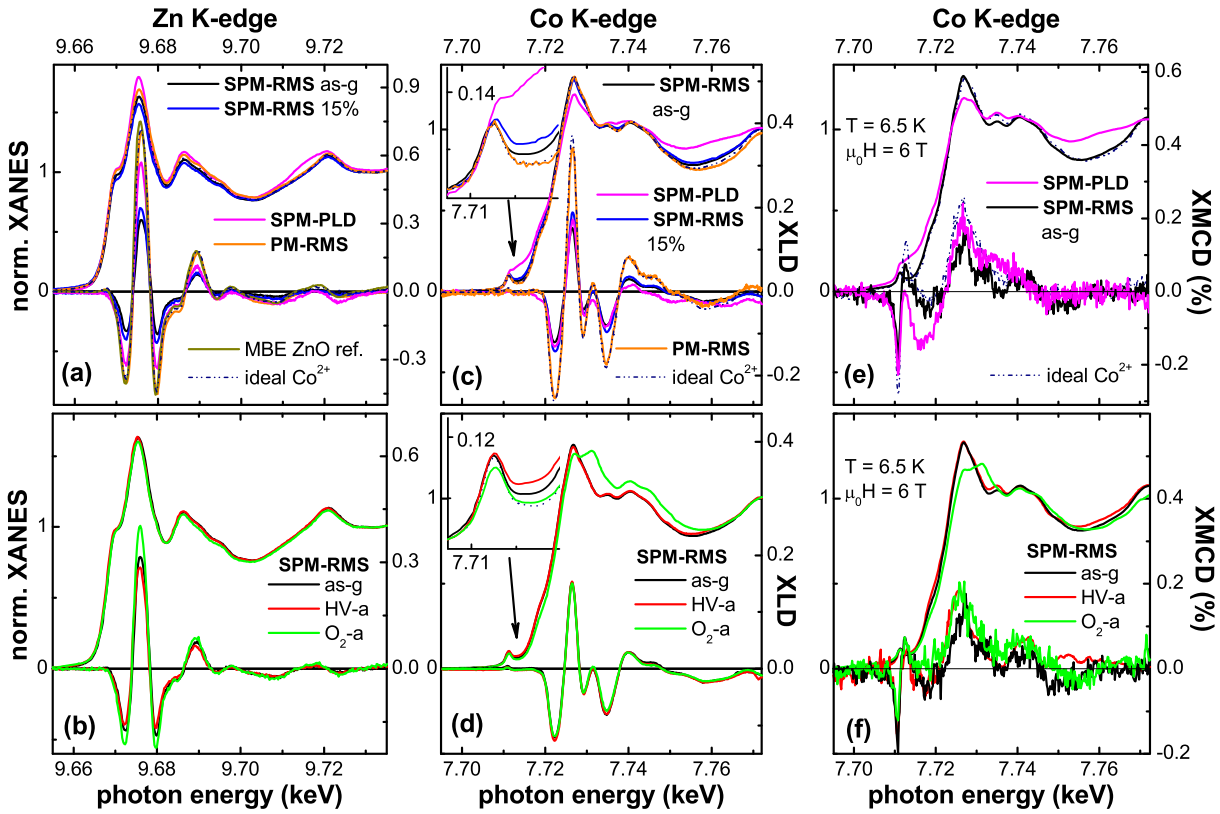

Figure 4. Detailed characterization of all specimens using hard XAS. (a) Comparison of the XANES and the respective XLD at the Zn K-edge of the PM-RMS sample with those of the SPM-RMS and SPM-PLD samples. Two other reference specimens are also shown. The influence of annealing on the SPM-RMS specimen is shown in (b) for XANES and XLD at the Zn K-edge. (c) The same samples as in (a) but recorded at the Co K-edge; the inset enlarges the pre-edge feature characteristic of Co^{2+} in tetrahedral coordination. (d) The evolution of the Co K-edge XANES and XLD for the SPM-RMS sample after annealing. (e) XANES and respective XMCD spectra for the two SPM samples compared with a PM reference ('ideal Co^{2+}') at the Co K-edge. The influence of the annealing on the SPM-RMS is shown in (f).

line in figure 4(a). The size of the XLD signal (peak-to-peak signal between the first (down) and second (up) extremum) for this sample is 1.155 after the effects of self-absorption for this 305 nm thick film have been corrected. This can be compared to a reference Co : ZnO sample grown by RMS, which was discussed earlier [11] and is shown as a dash-dotted line ('ideal Co^{2+}') in figure 4. This sample yields a maximum XLD signal of 1.11; since it was only 144 nm thick, no self-absorption correction was made. This is by 4% smaller than the MBE sample, but comparable with the high-quality PLD sample in [8], which yields an XLD of 1.07 at the Zn K-edge. It should be noted that all Co : ZnO samples have slightly shifted ZnO(0002) reflections in XRD compared with undoped ZnO, which can be ascribed to small lattice distortions due to the Co doping, which may account for small deviations of a few per cent in the Zn XLD. The quality indicator (size of the Zn XLD) can now be compared with the samples discussed in this paper.

The PM-RMS sample shown in figure 1 yields an XLD signal at the Zn K-edge of 1.11 and can thus be considered to be of high crystalline perfection, which is consistent with the findings of TEM analysis in figure 1. Note that the size of the XLD is obviously not strongly influenced by the columnar microstructure as long as the columns are of good crystalline quality and well oriented. Such high-quality samples in the thickness range of 100 nm as shown in figure 4(a) and in [8, 11] typically have an FWHM of the ZnO(0002) reflection of less than $\sim 0.13^\circ$ in XRD measurements.

In contrast, the SPM samples exhibit a reduced XLD at the Zn K-edge, indicative of lesser structural quality. Whereas the SPM-PLD sample exhibits an XLD signal of 0.90 and thus largely maintains good crystallinity, the two SPM-RMS samples have a clearly reduced XLD of 0.58 for the SPM-RMS 15% sample and of 0.49 for the SPM-RMS sample. The comparison of the reduced XLD with the TEM analysis in figure 2 demonstrates that a reduction of the XLD by a factor of more than two is correlated with the presence of many rotated grains and poor structural integrity. The remaining XLD signal most likely stems from the bottom part of the film close to the substrate, but some of the rotated grains may also be oriented so that they contribute to the XLD. Figure 4(b) shows the evolution of the Zn K-edge XLD for the SPM-RMS upon annealing. Whereas high-vacuum annealing reduces the XLD slightly to 0.44, O_2 annealing increases it to 0.62, which correlates well with the fact that this sample was prepared under oxygen-deficient conditions. Although oxygen annealing turns the sample PM, the crystalline quality is not fully re-established compared with the PM samples.

Figures 4(c) and (d) show XANES and XLD spectra of the same samples as in (a) and (b), respectively, but now measured at the Co K-edge. The insets enlarge the pre-edge feature of the Co K-edge characteristic of Co^{2+} in tetrahedral coordination, which was used as a quality indicator earlier [11]. In figure 4(c), it becomes obvious that the PM-RMS sample and the reference specimen (ideal Co^{2+}) have a virtually identical Co K-edge XLD of 0.62 and 0.63, respectively, which can be compared to the 0.67 for the high-quality PLD sample in [8]. Also, the shape of the pre-edge feature for these samples is virtually identical, pointing toward Co being fully Co^{2+}. In contrast, all SPM samples have an XLD signal of about 0.28(2), i.e. a reduction by a factor of more than two irrespective of the size of the Zn K-edge XLD. This indicates that the substitutional Co incorporation can be to some degree independent of the structural perfection of the ZnO host crystal. For all SPM samples, the pre-edge feature is less pronounced compared to the PM samples, which is indicative of increasing metallic character of the Co species from the SPM RMS as-g over the SPM-RMS 15% to the SPM-PLD sample.

Figure 4(d) shows the evolution of XANES and XLD of the SPM-RMS sample upon annealing. Surprisingly, the size of the Co K-edge XLD does not significantly change upon any annealing procedure. Obviously, the fraction of Co atoms (which are incorporated in the substitutional lattice site and thus give rise to the XLD signal) is not altered by the annealing. Therefore, the fraction of substitutional Co cannot be responsible for the change in magnetic properties as measured by SQUID in figure 3. However, there is an obvious change in the shape of the XANES for the SPM-RMS O_2-a sample. The maximum of the absorption is clearly shifted to a higher photon energy, which is indicative of another Co species (with a higher oxidation state than 2+) being present in this particular sample. Also, the pre-edge region (figure 4(d), inset) reveals significant changes upon annealing: the high-vacuum annealing decreases the pre-edge feature indicative of increasing metallicity of the Co, whereas the oxygen annealing leads to a pre-edge feature that is almost identical to the ideal Co^{2+} (dash-dotted line). Obviously, non-substitutional Co, i.e. Co without a sizable XLD signature (such as Co metal, cubic CoO, etc), is responsible for the change in magnetic properties upon annealing.

Figure 4 also shows the Co-specific magnetic properties as measured using XMCD at the Co K-edge at 6.5 K in an external magnetic field of 6 T for all SPM samples (e) and the changes upon annealing (f). As introduced before, ideal Co^{2+} has zero XMCD signal at 7718.26 eV, where Co metal has its maximum dichroic signal [11]. The maximum XMCD signal of ideal Co^{2+} at the pre-edge feature is in turn at 7711.35 eV; however, metallic Co also has a finite XMCD signal at this photon energy, so that a superposition of both species can be measured there. In figure 4(e), it is obvious that at 7718.26 eV there is a sizable XMCD signal for the SPM-RMS sample, which is much more pronounced for the SPM-PLD sample. For the SPM-RMS sample this 'metallic' XMCD signal increases upon high-vacuum annealing, whereas it vanishes upon oxygen annealing (f). Oxygen annealing also reduces the size of the XMCD signal at the pre-edge feature, i. e. the overall magnetization, consistent with the SQUID measurements in figure 3(a).

The comprehensive analysis using XAS in figure 4 can be further refined on a quantitative basis. First, one can compare the size of the XLD at the Zn and Co K-edges of the SPM-RMS sample with the ideal Co^{2+} sample: whereas the Zn XLD is reduced to 44.4% of the ideal value, the Co XLD is reduced to 43.0%, i.e. in the most optimistic case of a correlated reduction of Zn and Co XLD, at least 3% of the Co as lower bound can be present as Co species with no significant XLD; the upper bound is naturally 57%. To put this crude estimate on more solid grounds, the Co K-edge XANES spectra are more suitable for such an estimate, because they capture all existing Co species that may be present in the sample. Note that hard x-rays can probe the entire thickness (about 100 nm) of the film without significant self-absorption effects [11]. Figure 5 displays fits of the measured XANES spectra for the SPM-RMS sample in the as-grown state (a), after high-vacuum (b) and oxygen annealing (c) using the reference spectra for ideal Co^{2+}, Co metal, Co_3O_4 and CoO shown in (d). Figure 5 includes the difference between experimental XANES and fit (thin lines), which was minimized by varying the content of the respective species in 1% steps, which is therefore a measure of the uncertainty of this procedure ($\pm 1\%$). The use of CoO XANES did not improve any of the fits; therefore it is excluded that a significant amount ($>1\%$) of (cubic) CoO is present in any sample. The SPM-RMS as-g (a) and HV-a (b) samples could be best fitted with a superposition of ideal Co^{2+} and Co metal XANES, revealing that in the as-grown state the sample contains 5% metallic Co, which is increased to 8% upon high-vacuum annealing. This increase is in good quantitative agreement with the increase of the saturation value of the magnetization at 300 K as measured by SQUID in figure 3(a). The SPM-RMS O_2-a could be fitted with a combination of 57% of ideal Co^{2+} and 43% of Co_3O_4 without a significant amount of metallic Co, again consistent with zero magnetization at 300 K as measured by SQUID. Since Co_3O_4 is an antiferromagnet with a Néel temperature of 40 K [29], this naturally explains the absence of any SPM signatures and the reduction of the magnetization by a factor of more than two at 5 K as measured by SQUID in figure 3(a). Note that Co and Co_3O_4 as secondary phases have also been found earlier by selected area electron diffraction in polycrystalline Co : ZnO films [30] in line with the present XAS analysis.

The quantitative analysis can be further refined, which will be exemplified using the SPM-RMS as-g sample. Using the hypothesis that the SQUID response at 300 K of this sample is solely due to the 5% fraction of metallic Co (with a magnetic moment of $1.73\mu_B$ atom^{-1}), one can estimate the expected magnetization at 5 K and 4 T in the SQUID experiment. For this discussion the unit emu is used in the following, since this is the unit directly provided by the SQUID. If 5% metallic Co give rise to 1.28×10^{-5} emu under fully saturated conditions,

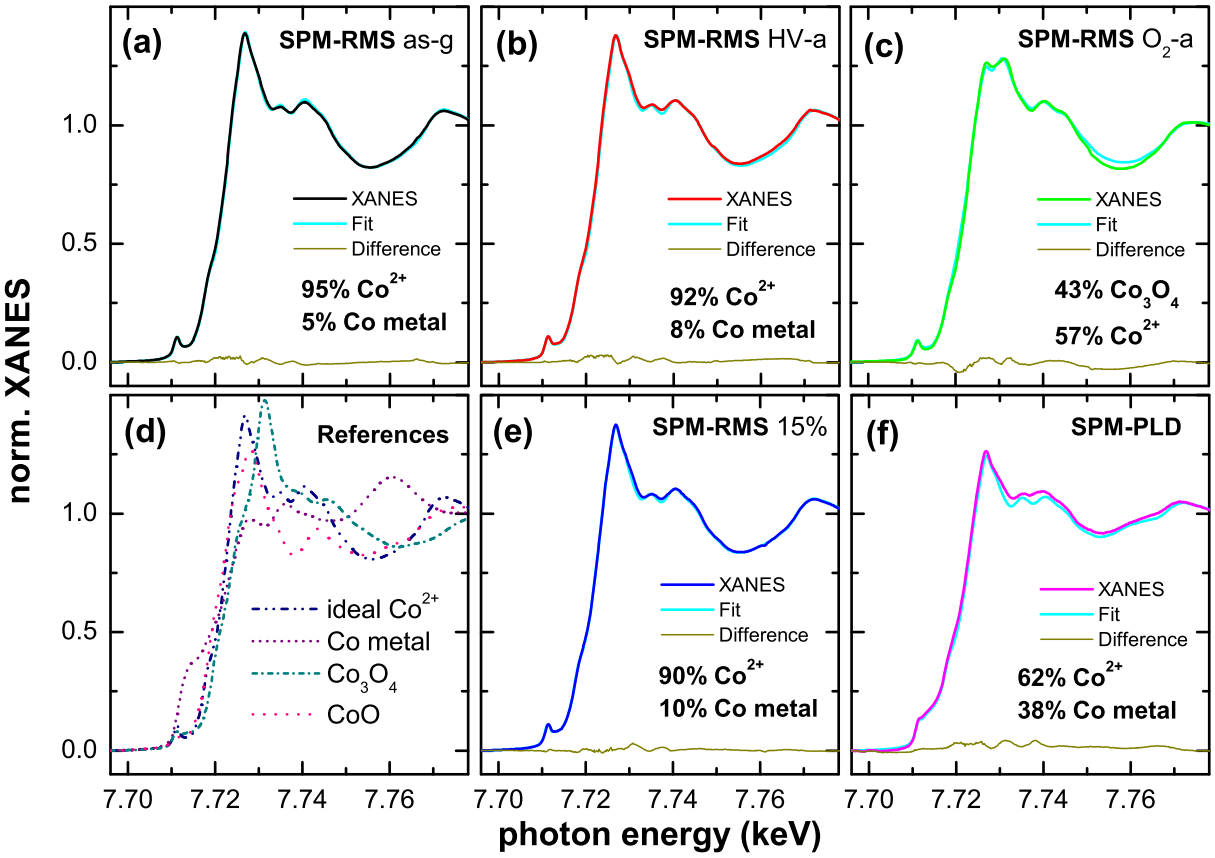

Figure 5. Quantitative analysis of the XANES of the SPM-RMS specimen in the as-grown state (a) and after annealing under high vacuum (b) and oxygen atmosphere (c), together with a fit using the reference spectra for ideal Co^{2+}, Co metal, Co_3O_4 and CoO shown in (d) and the respective difference between experiment and fit (thin lines). The same fitting is shown for the SPM-RMS 15% sample (e) and the SPM-PLD sample (f), revealing a significant amount of metallic Co.

100% Co give 2.56×10^{-4} emu, i.e. 2.43×10^{-4} emu for the remaining 95% Co if these have $1.73\mu_B$ as well. Since it is known that the ideal Co^{2+} possesses a magnetic moment of $3.41\mu_B$ (see [7, 24]), i.e. double the moment of metallic Co, 4.86×10^{-4} emu can be expected in full magnetic saturation. Since this moment is of PM nature, as seen in figure 3(a), the value has to be corrected for the experimental measurement conditions yielding an expected signal of 3.81×10^{-4} emu at 5 K and 4 T, while the SQUID experiment exhibits 7.75×10^{-5} emu, i.e. only about 20% of the expected value. Based on a statistical dopant distribution, such a reduction stems from antiferromagnetic coupling of Co–O–Co pairs in these samples and is known to depend on the actual Co concentration in the sample [7, 8]. Using this relation, the reduction can be correlated with a dopant concentration by assuming that only the isolated Co dopant atoms contribute to the SQUID signal. For the derived value of 20% of the expected signal, this can be associated with a dopant concentration of about 12.5%, which is consistent with the nominal concentration of 10% in this particular sample, as well as with the TEM analysis of the homogeneous regions in figure 6 below. The preceding quantitative estimate indicates that it is

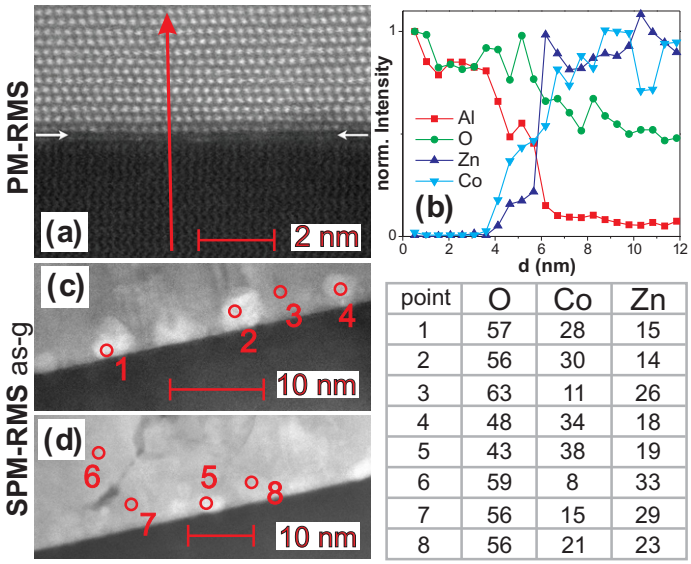

point	O	Co	Zn
1	57	28	15
2	56	30	14
3	63	11	26
4	48	34	18
5	43	38	19
6	59	8	33
7	56	15	29
8	56	21	23

Figure 6. (a) High-resolution, aberration-corrected STEM high-angular annular dark field (HAADF) image of the interface of the PM-SPM film and the sapphire substrate. (b) EDS of Al (red squares), O (green circles), Zn (blue up triangles) and Co (cyan down triangles) along the red line shown in (a). (c, d) Elemental analysis using EDS at two different spots of the SPM-RMS as–g sample. The table summarizes the concentration of O, Co and Zn in % on some crystallites (1, 2, 4, 5 and 8), as well as on the homogeneous part of the film (3, 6 and 7). The ADF inner detector semi-angles used were (a) 59.8 mrad and (c, d) 47.4 mrad.

quantitatively possible that the SQUID signal at 300 K can be solely caused by the metallic Co fraction in this sample, but it does not constitute an unambiguous proof.

Turning back to the fit of the XANES spectra of the SPM-RMS 15% sample in figure 5(e) and the SPM-PLD sample (f), one sees that the SPM-RMS 15% sample contains 10% metallic Co, whereas the SPM-PLD sample contains 38% metallic Co. The latter value has a larger uncertainty of about ±3% due to the lesser quality of the fit, which can either reproduce the pre-edge region well, or the main absorption. Using the derived metallic fraction, a comparable analysis as that for the SPM-RMS as-g sample above can be performed based on the SQUID measurements (see figure 7) and yields an estimated Co concentration of 6.6% for the SPM-PLD (nominally 5%) and of 11.5% for the SPM-RMS 15% sample. The latter discrepancy may be due to the fact that the peak in the ZFC curve of the SPM-RMS 15% is much broader, especially down to low temperatures (not shown), which indicates that very small clusters may be present in this particular sample, leading to a small supermoment which cannot be fully saturated with 4 T at 300 K, and therefore being subtracted together with the diamagnetic background. In addition, it was shown for nominally 15% Co : ZnO PM samples that the presence of larger Co–O–. . .-configurations leads to an increased contribution to the $M(T)$ behavior beyond the isolated Co atoms compared to nominally 10% Co : ZnO samples [24]—this would also account for the discrepancy between estimated and nominal Co concentrations in the SPM-RMS 15% sample following the above procedure. Nonetheless, for all SPM samples the above estimation does not preclude the possibility that the SQUID signal at 300 K is only caused by the metallic fraction of the Co dopant.

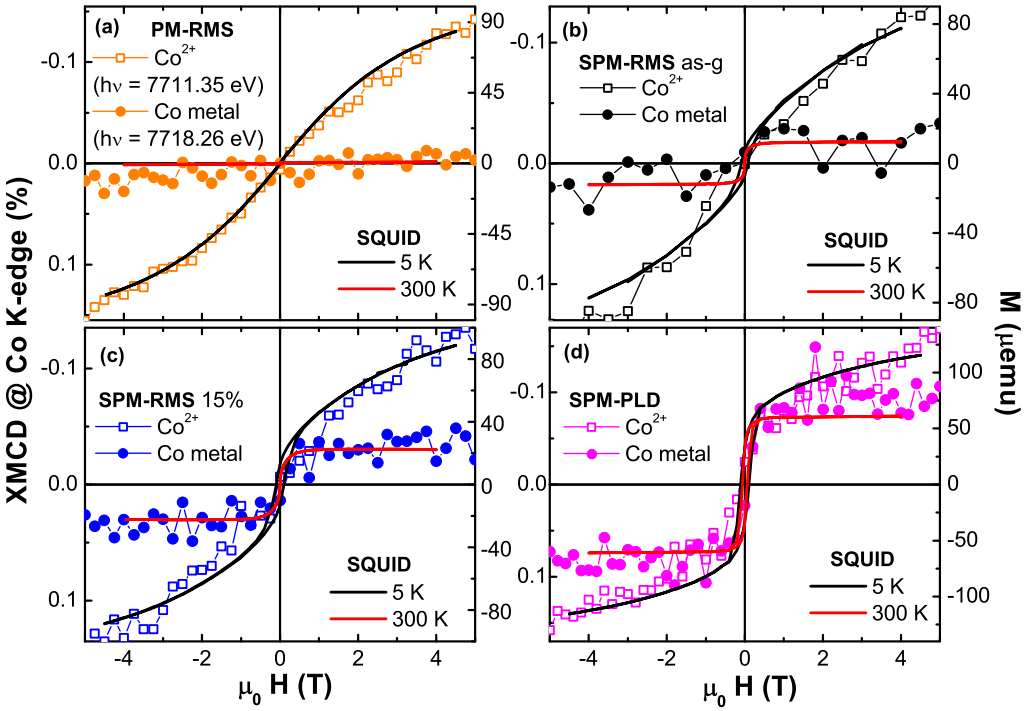

Figure 7. Element-specific $M(H)$ curves recorded at two different photon energies characteristic of Co^{2+} (open squares) and metallic Co (full circles) at 6.5 K in comparison to $M(H)$ curves at 5 K (black line) and 300 K (red line). Data are shown adjusted to each other for the PM-RMS (a), the SPM-RMS (b), the SPM-RMS 15% (c) and the SPM-PLD (d).

3.4. Elemental analysis using TEM

Figure 6 compares the distribution of the Co dopant atoms in the PM-RMS sample (panels (a) and (b)) with that in the SPM-RMS as-g sample (panels (c) and (d)). In figure 6(a), a high-resolution aberration-corrected STEM HAADF image of the interface between the Co : ZnO film and the sapphire substrate is shown, revealing the good crystalline order of the PM-RMS sample. An elemental analysis using EDS was done across the interface along the red line in (a), and the normalized concentrations of Al (red squares), O (green circles), Zn (blue up triangles) and Co (cyan down triangles) are shown in (b). Both the STEM image and the EDS indicate that about three (at most five) atomic layers at the interface are intermixed. Above that 1–2 nm wide interface region (less than 1–2% of the entire film thickness of 158 nm), the Co distribution is rather homogeneous, confirmed by further EDS line scans, which were also taken across the grain boundaries (not shown). In contrast, the SPM-RMS as-g sample shows a very inhomogeneous Co distribution at various spots of the sample shown in figures 6(c) and (d). The elemental analysis of different points (labeled by numbers and provided in % with an experimental uncertainty of a few per cent) is summarized in the table in figure 6. As a general trend, one sees that the entire film appears to be slightly oxygen-rich. Further, one has to discriminate between rather homogeneous areas of the sample with no obvious rotated grains, e.g. spots 3, 6 and 7, where the measured Co concentration is around the nominal value of 10%. These areas presumably give rise to the PM fraction of the Co also being responsible for the

XLD signal at the Co K-edge. In areas where clear crystallites are visible (spots 1, 2, 4, 5 and 8), the Co concentration is drastically increased above 20% to 38%. Further, it can be seen that at points where the Co concentration rises above 30% (spots 4 and 5), the oxygen content is less than 50%, i.e. in these oxygen-deficient areas it is possible that a fraction of the Co is metallic, which can account for the 5% metallic Co derived from the XANES analysis in figure 5(a). In these regions of oxygen deficiency it is reasonable to assume that the Zn is also underoxidized so that by annealing in high vacuum the Co is further reduced by the Zn, leading to a net increase of the metallic fraction, as seen in figures 4(f) and 5(b). In contrast, annealing in oxygen leads to complete oxidation of the metallic Co fraction, thus causing the SPM properties to vanish. The globular structure of the film seen in figure 2 facilitates the oxygen penetrating deep into the layer to oxidize about half of the Co to form Co_3O_4, as seen by XANES in figure 5(c). The elemental composition and microstructure found by TEM is therefore consistent with the observed annealing behavior of the SPM-RMS sample.

3.5. Origin of the SPM behavior

All the results presented so far point towards an extrinsic origin of the SPM behavior, caused by small precipitations of metallic Co present in the samples. Despite a strong influence of annealing procedures, it has been demonstrated that the magnetic properties are altered by modifying the chemical state of a fraction of the Co being present in its metallic form, as evidenced by XAS. The question remaining to be addressed is whether this also holds on a quantitative basis and whether the $M(H)$ curve at 300 K indeed stems from this metallic fraction of the Co dopant atoms. To establish this correlation, one can take advantage of the chemical sensitivity of the XMCD. As pointed out above, one can measure the magnetic response of metallic Co at the Co K-edge at a different photon energy (7718.26 eV) than the overall magnetic response of Co (7711.35 eV). Therefore, XMCD(H) curves have been recorded at these two characteristic photon energies at 6.5 K. The resulting data are shown in figure 7 for the PM-RMS (a), the SPM-RMS as-g (b), the SPM-RMS 15% (c) and the SPM-PLD (d) samples, together with the respective $M(H)$ curves measured by SQUID at 5 and 300 K, respectively. XMCD and SQUID data have separate vertical axes, which were scaled to match the data with each other. Although the XMCD data are rather noisy due to the small dichroic signal ($<$0.3%), it can be seen that for the PM-RMS sample no XMCD signal is present for metallic Co, which coincides with no sizable magnetization at 300 K, as measured by SQUID. In contrast, the 5 K SQUID data match the XMCD data at the pre-edge (all Co species) rather well. This analogy holds for all three SPM samples as well, i.e. the metallic Co XMCD(H) curve measured at 6.5 K always coincides with the SQUID $M(H)$-curve at 300 K, i.e. it quickly saturates with magnetic field and essentially remains constant. The constant XMCD signal at the metallic photon energy has been verified up to 17 T for the SPM-RMS as-g sample; however, figure 7(b) shows only the field range accessible to the SQUID.

Figure 7 directly suggests that the metallic Co fraction can fully account for the observed SPM behavior based on two assumptions that shall be briefly discussed. (i) The total magnetic response can be reliably measured at the pre-edge (7711.35 eV). (ii) The temperature dependence of the magnetization of the metallic Co can be neglected between 6.5 and 300 K. Assumption (i) can be justified as follows: comparing the size of the XMCD signal at 7711.35 eV (figure 4(b) in [11]), one sees that the XMCD of Co metal is about half that of the ideal Co^{2+}. On the other hand, only a fraction of $\sim$30% of the Co atoms contribute to the

magnetic signal due to the antiferromagnetic compensation of the Co–O–Co pairs [7, 8]. These two facts lead to the situation that metallic Co and ideal Co^{2+} contribute equally (within the necessary accuracy for this comparison) to the XMCD signal. One should note that especially at low magnetic fields where the XMCD is even smaller, the experimental uncertainty is rather large, so that the hysteretic behavior cannot be reliably resolved at the Co K-edge. Assumption (ii) is also a reasonable assumption. The drop in magnetization from 30 to 300 K has been measured by *in situ* SQUID magnetometry for epitaxial Co films (figure 3(a) of [31]). It has been shown that above film thicknesses of eight atomic layers, i.e. about 1.4 nm, this reduction is below a few per cent because the reduction of the Curie temperature compared to bulk Co due to finite-size effects is sufficiently small. Although the finite-size effects for nanocrystallites may be slightly different from those for ultrathin films, it is unlikely that the Co-rich clusters seen by TEM in figures 2(b) and 6(c) and (d), which are of the order of 3–5 nm or larger, have a more pronounced reduction of the Curie temperature and thus a stronger reduction of the magnetization between 6.5 and 300 K than a 1.8 nm film between 30 and 300 K. Therefore, the suggestive character of the correlation between the 300 K SQUID data and the metallic Co fraction should also hold on a quantitative basis.

4. Conclusion

In summary, we have used a comprehensive set of experimental techniques for an in-depth characterization of a range of Co : ZnO samples grown mostly by RMS. We were able to associate a certain degree of the measured XLD at the Zn and Co K-edges with the high structural quality seen in TEM investigations, as well as by comparing to an MBE ZnO reference sample. These findings are compared with SPM samples in order to clarify the microscopic origin of the SPM behavior found by integral SQUID magnetometry. XLD as well as TEM reveals a drastic loss in structural quality, which is accompanied by a fraction of Co dopant atoms being metallic in all SPM samples. The elemental analysis using XAS and TEM can also explain the observed changes of the magnetic properties upon annealing procedures, which is not caused by a change in the carrier concentration of the DMS, but is merely a consequence of reduction or oxidation of the metallic fraction of the Co dopant atoms. The various Co-containing species could be quantified by fitting the XANES using reference spectra, which in turn are quantitatively consistent with the magnetization values measured by SQUID. Finally, it could be directly shown by comparing integral SQUID magnetometry with element-specific XMCD(H) measurements that the metallic Co species found in all SPM samples by means of their spectroscopic signatures indeed causes the SPM behavior of Co : ZnO. In turn, these findings underline that the spectroscopic signatures of phase pureness in XANES, XLD and XMCD are a meaningful and quantitative measure to characterize a range of oxide-based DMS samples, in agreement with the complementary finding of an in-depth TEM analysis.

Acknowledgments

AN gratefully acknowledges financial support from the German Research Foundation (DFG) through the Heisenberg Programme. The early stage of this work was supported by the European Commission under grant number MEXT-CT-2004-014195. The TEM investigations were supported by the ‘FunDMS’ Advanced Grant of the European Research Council within the ‘Ideas’ 7th Framework Programme of the European Commission. We are grateful to T Wassner

and M Eickhoff from the Walter Schottky Institute, Garching, for providing us with the MBE-grown ZnO film and to M Gacic and G Jakob from the Johannes Gutenberg University, Mainz, for providing us with the SPM-PLD sample.

References

[1] Dietl T 2010 *Nat. Mater.* **9** 965
[2] Ueda K, Tabata H and Kawai T 2001 *Appl. Phys. Lett.* **79** 988
[3] Chambers S A 2010 *Adv. Mater.* **22** 219
[4] Ogale S B 2010 *Adv. Mater.* **22** 3125
[5] Kittilstved K R, Schwartz D A, Tuan A C, Heald S M, Chambers S A and Gamelin D R 2006 *Phys. Rev. Lett.* **97** 037203
[6] Ney V, Ye S, Kammermeier T, Ney A, Zhou H, Fallert J, Kalt H, Lo F-Y, Melnikov A and Wieck A D 2008 *J. Appl. Phys.* **104** 083904
[7] Sati P, Deparis C, Morhain C, Schäfer S and Stepanov A A 2007 *Phys. Rev. Lett.* **98** 137204
[8] Ney A, Ollefs K, Ye S, Kammermeier T, Ney V, Kaspar T C, Chambers S A, Wilhelm F and Rogalev A 2008 *Phys. Rev. Lett.* **100** 157201
[9] Ney A, Ney V, Ye S, Ollefs K, Kammermeier T, Kaspar T C, Chambers S A, Wilhelm F and Rogalev A 2010 *Phys. Rev.* B **82** 041202
[10] Ney A 2010 *Materials* **3** 3565
[11] Ney A *et al* 2010 *New J. Phys.* **12** 013020
[12] Barla A *et al* 2007 *Phys. Rev.* B **76** 125201
[13] Tietze T, Gacic M, Schütz G, Jakob G, Brück S and Goering E 2008 *New J. Phys.* **10** 055009
[14] Xu Q, Schmidt H, Hartmann L, Hochmuth H, Lorenz M, Setzer A, Esquinazi P and Grundmann M 2007 *Appl. Phys. Lett.* **91** 092503
[15] Straumal B B, Mazilkin A A, Protasova S G, Myatiev A A, Straumal P B, Schütz G, van Aken P A, Goering E and Baretzky B 2009 *Phys. Rev.* B **79** 205206
[16] Coey J M D, Mlack J T, Venkatesan M and Stamenov P 2010 *IEEE Trans. Magn.* **46** 2501
[17] Park J H, Kim M G, Jang H M, Ryo S and Kim Y M 2004 *Appl. Phys. Lett.* **84** 1338
[18] Opel M, Nielsen K-W, Bauer S, Goennenwein S T B, Cezar J C, Schmeisser D, Simon J, Mader W and Gross R 2008 *Eur. Phys. J.* B **63** 437
[19] Rode K *et al* 2008 *Appl. Phys. Lett.* **92** 012509
[20] Deka S and Joy P A 2006 *Appl. Phys. Lett.* **89** 032508
[21] Rogalev A, Goulon J, Goulon-Ginet C and Malgrange C 2001 *Lect. Notes Phys.* **565** 61
[22] Ney A, Kammermeier T, Ney V, Ollefs K and Ye S 2008 *J. Magn. Magn. Mater.* **320** 3341
[23] Sawicki M, Stefanowicz W and Ney A 2011 *Semicond. Sci. Technol.* **26** 064006
[24] Ney A, Kammermeier T, Ollefs K, Ye S, Ney V, Kaspar T C, Chambers S A, Wilhelm F and Rogalev A 2010 *Phys. Rev.* B **81** 054420
[25] Estle T L and de Wit M 1961 *Bull. Am. Phys. Soc.* **6** 445
[26] Sati P *et al* 2006 *Phys. Rev. Lett.* **96** 017203
[27] Coey J M D, Venkatesan M and Fitzgerald C B 2005 *Nat. Mater.* **4** 173
[28] Gacic M, Adrian H and Jakob G 2008 *Appl. Phys. Lett.* **93** 152509
[29] Roth W L 1964 *J. Phys. Chem. Solids* **25** 1
[30] Deka S, Pasricha R and Joy P A 2006 *Phys. Rev.* B **74** 033201
[31] Ney A, Poulopoulos P, Farle M and Baberschke K 2000 *Phys. Rev.* B **62** 11336